Qubit fidelity distribution under stochastic Schrödinger equations driven by classical noise

R. J. P. T. de Keijzer,[1,2,*] L. Y. Visser,[2,3] O. Tse,[2,3] and S. J. J. M. F. Kokkelmans[1,2]
[1]Department of Applied Physics, Eindhoven University of Technology, P. O. Box 513, 5600 MB Eindhoven, The Netherlands
[2]Eindhoven Hendrik Casimir Institute, Eindhoven University of Technology, P. O. Box 513, 5600 MB Eindhoven, The Netherlands
[3]Department of Mathematics and Computer Science, Eindhoven University of Technology, P. O. Box 513, 5600 MB Eindhoven, The Netherlands

(Received 22 January 2024; accepted 18 March 2025; published 16 April 2025)

Environmental noise affecting controlled quantum systems is typically described by a dissipative Lindblad equation, which captures the system's average state through the density matrix ρ. One approach to deriving this equation involves a stochastic operator evolving under white noise in the Schrödinger equation; however, white noise fails to accurately depict real-world noise profiles, where lower frequencies often dominate. This study proposes a method to determine the *analytic distribution* of qubit fidelities in significant stochastic Schrödinger equation scenarios, with qubits evolving under more realistic noise profiles such as *Ornstein-Uhlenbeck* noise. This method enables the prediction of the mean, variance, and higher-order moments of qubit fidelities, offering insights crucial for assessing permissible noise levels in prospective quantum computing systems and guiding decisions about control systems procurement. Additionally, these methodologies are essential for optimizing qubit state control affected by classical control system noise.

DOI: 10.1103/PhysRevResearch.7.023063

I. INTRODUCTION

To realize their potential in tackling highly complex simulation and optimization tasks, quantum computers must reliably execute numerous successive operations, effectively manipulating qubits with high fidelity. However, in the current era of noisy intermediate-scale quantum computing [1], quantum systems contend with noise originating from various sources. These include uncontrollable factors such as radiative decay as well as noise introduced by control systems, such as fluctuations in laser frequency and intensity [2–4].

Although one approach to mitigating control noise involves improving system quality, this often involves substantial monetary and technological complexities. Alternatively, designing control operations resistant to such noise. sources offers a pragmatic strategy to minimize their impact [5,6]. Thus, it is crucial to have a complete understanding of the effects that various realistic control noise profiles may have on the evolution of the qubit, which is the main issue addressed in this work. We believe that this understanding can inform the development of effective control strategies necessary to improve quantum computing capabilities and to tackle the challenges caused by noise, ultimately leading to more reliable and advanced systems.

Noisy quantum systems are commonly treated as open systems whose density matrices ρ evolve under the Lindblad master equation [7]. These equations describe the effective Markovian behavior of an open quantum system and can be derived by various approaches [8] (cf. Sec. II A for an example). However, the assumption of strict Markovianity is often deemed unrealistic, particularly in scenarios that involve colored control noise. In such cases, lower frequencies tend to dominate the power spectral density [9], rendering the Markovian assumption inadequate for accurately describing the dynamics of the system. Moreover, while a density matrix captures essential aspects of a system's state, it does not fully characterize it, as different ensembles of states $\{\psi_j\}_j$ may share a common density matrix $\rho = \mathbb{E}[\psi_j \psi_j^\dagger]$ [10]. This ensemble of (stochastic) states $\{\psi_j\}_j$ is often called a *unraveling* of the density matrix and is useful in Monte Carlo simulations of open quantum systems [11]. Moreover, the complete ensemble contains more information than the density matrix ρ alone [12], offering valuable insights on correlations between state distributions and noise effects, see Fig. 1. Such information has the potential to be used to devise error mitigation strategies [13,14]. For example, a Markovian ensemble of states $\{\psi_j\}_j$ may be described by the stochastic Schrödinger equation (SSE) [15], where classical stochasticity is introduced through white noise processes.

Efforts are being made to find generalizations of the SSE in the non-Markovian regime while possessing a reasonable physical interpretation. One method for achieving this involves generalizing the Markovian Lindblad approaches in Ref. [16] to non-Markovian master equations [17] and finding physically meaningful unravelings, as demonstrated for jump processes in Ref. [18]. In contrast, we leverage the approach in Ref. [19] and start from a generalized SSE. In this setting, the foundation for non-Markovian behavior is introduced via a random Hamiltonian method with control functions displaying colored noise. This framework naturally leads to an unraveling that maintains a coherent measurement interpretation.

*Contact author: r.j.p.t.d.keijzer@tue.nl

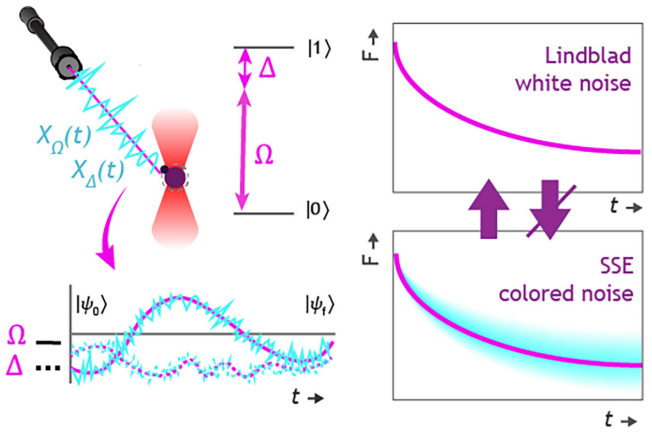

FIG. 1. Illustration of control system laser noise, denoted by X^Ω and X^Δ, impacting the qubit Rabi frequency Ω and detuning Δ and leading to a loss of fidelity F. The SSE can be used to find a distribution of fidelities subjected to colored noise, including white noise. Conversely, the Lindblad equation is only valid for white noise and results in an average fidelity rather than the full fidelity distribution.

Subsequently, the non-Markovian master equation may be inferred, as outlined in Ref. [20].

In a noisy quantum system, both classical control noise and thermal noise from the environment [21] affect the qubit fidelity on different levels, depending on the qubit architecture [22]. Fixing one type of noise gives a stochastic unravelling of the Lindblad equation. In the case of control noise, it is possible to get experimental data on the individual realizations of the noise. However, measuring the thermal noise is more complicated, as the destruction of the qubit state after measurements ensures one can only directly measure the average effect of thermal noise as given by the Lindblad equation, making it impossible to verify whether the corresponding individual realizations match with the theoretical unravelling. In this work, we limit our analysis to classical noise affecting the qubit control functions, such as laser intensity and frequency noise, based on the semiclassical treatment of light-atom interactions [23,24]. The non-Markovian SSE (hereafter referred to as SSE) captures the full state distribution with respect to a broad spectrum of control noise profiles, offering multifaceted advantages, when compared to Markovian density matrix methods. First, leveraging SSE enables accurate predictions of qubit fidelities, essential for ensuring system compliance with specified tolerance thresholds before procurement. Second, SSE facilitates precise responses to qubit system control noise [25–27] as it accounts for noise influence during each shot-to-shot state preparation, instead of an average response. Last, understanding how noise impacts fidelity distributions proves vital for error correction strategies, which can exploit noise-fidelity correlations to correct for minor perturbations [13]. To summarize, the relationships between noise and fidelity established in this work enable straightforward identification and exclusion of individual state preparations that fall short of predefined fidelity benchmarks.

Using our approach, we highlight several significant scenarios of classical control noise that impact qubits, and we derive the corresponding closed stochastic differential equations (SDEs), which can be solved either analytically or numerically to find the fidelity distribution based on various types of noise spectra. This includes PI controller-like processes that are useful for error mitigation (as detailed in Sec. II B 6). We further validate these SDE systems against Monte Carlo simulations. Notably, our numerical simulations based on the SDE systems offer a simpler and more efficient alternative to the Monte Carlo methods previously reported in Ref. [28].

A. Relation to previous work

This work aligns with other studies that have examined the influence of noise on qubit fidelity [29–31]. These studies primarily operate within the framework of the Lindblad equation and mainly focus on the small noise regime. However, the Lindblad equation's utility is limited to analyzing the mean fidelity, as it does not provide a comprehensive view of the entire fidelity distribution of qubits.

Likewise, previous studies on the SSE for quantum computing [32–34] have primarily produced lower bounds or approximations for achievable qubit state preparation fidelities, typically addressing white noise and mean fidelities. These analyses could have been carried out using the Lindblad equation. However, the correlations provided by the fidelity distribution are particularly relevant in error-correcting scenarios, where it is critical to ensure that every state preparation closely aligns with the intended state for effective error correction.

Additionally, our SSE method is inherently normalized and requires normalization primarily to account for numerical errors. This differentiates it from approaches that rely on the standard Schrödinger equation with a stochastic Hamiltonian [2,27,35–37], which provide accurate results only under certain conditions (refer to Appendix A).

Noise mitigation has also been addressed in related work through specific recovery operations, particularly in the context of low-frequency noise [14,23]. Our methods can facilitate real-time noise mitigation, offering a potential complement to postprocessing recovery operations. Furthermore, this study establishes a basis for extending to general operators and noise profiles. In summary, our developed methods offer several advantages over the state-of-the-art techniques:

(i) Exact expressions for fidelity distributions as functions of individual noise realizations, allowing verification and characterization of control systems;

(ii) Fidelity-noise correlations that are crucial for error mitigation;

(iii) Normalized methods for handling colored noise, unlike approaches based on the Lindblad equation or stochastic Hamiltonians;

(iv) Significant speed-ups in fidelity calculations.

The paper is structured as follows. Section II A provides an overview of the SSE, highlighting its connection to noise arising from control mechanisms and comparing it to the Lindblad equation under white noise. Section II B details our SDE-based methodology along with the numerical scheme used for solving the SSE equations. Section II C presents the initial findings of our model applied to single- and multiple-qubit systems, incorporating analyses of white noise, colored noise, and feedback processes.

II. RESULTS

A. Stochastic Schrödinger equation

The standard Schrödinger equation describing the evolution of a pure state ϕ is given by [38]

$$\mathrm{d}\phi = -iH(t)\phi\,\mathrm{d}t, \tag{1}$$

where $H(t)$ is a time-dependent Hamiltonian. Generic non-Markovian SSEs start by considering a linear equation for a non-normalized distribution of states ψ [19,28]

$$\mathrm{d}\psi = C\psi\,\mathrm{d}t + R\psi\,\mathrm{d}X_t,$$

Here $X = (X_t)_{t\geqslant 0}$ is a real-valued noise source described by an Itô process with finite quadratic variation [39,40]

$$[X]_t = \int_0^t \gamma_s^2\,\mathrm{d}s,$$

where γ is a predictable process that is integrable with respect to the white noise source [41,42]. As $|\psi|^2$ should represent a probability density, we require $\mathbb{E}[|\psi|^2] = 1$ at all times, imposing restrictions on C and R of the form (see Appendix A for derivation)

$$\mathrm{d}\psi = -iH\psi\,\mathrm{d}t - \tfrac{1}{2}S^\dagger S\psi\,\mathrm{d}[X]_t - iS\psi\,\mathrm{d}X_t, \tag{2}$$

where S is the noise operator. To simplify the presentation of our results, we focus on a single noise process and operator. However, the results can be extended straightforwardly to multiple independent noise processes and commuting noise operators. This class of stochastic evolution equations was introduced as a dissipative model without observation [19,28,43,44]. For $\rho = \mathbb{E}[\psi\psi^\dagger]$, a master equation with non-Markovian effects can be obtained. However, this will generally not be of closed form due to correlations between X_t and ψ_t [28]. Closed-form approximations can be obtained using the Nakajima-Zwanzig approach [45] but are out of the scope of this work.

In this work, the primary concern here is control noise in a laser system, as in a Rydberg system [46]. However, the methods can be applied to all classical driving systems for different qubit architectures, e.g., electrical currents in superconducting chips [47,48]. Most single qubit systems are controlled using a *coupling operator*,

$$H_{\mathrm{coup}} = e^{i\varphi}|0\rangle\langle 1| + e^{-i\varphi}|1\rangle\langle 0|,$$

and a *detuning operator*,

$$H_{\mathrm{det}} = (I - \sigma_Z)/2 = |1\rangle\langle 1|,$$

which in combination give the control Hamiltonian [25]

$$H(t) = \Omega(t)H_{\mathrm{coup}} + \tfrac{1}{2}\Delta(t)H_{\mathrm{det}},$$

where Ω is the Rabi frequency, φ is the phase, and Δ is the detuning. Because we limit ourselves to control noise, the noise operator S must inherently stem from the control Hamiltonian, resulting in the hermitian condition $S = S^\dagger$.

Possible noise sources are in the laser intensity, relating to Ω, frequency, relating to Δ, and phase φ. The pulses (including the classical noise sources) are then given by $\mathrm{d}\tilde{\Omega} = \Omega\mathrm{d}t + \mathrm{d}X^\Omega$, $\mathrm{d}\tilde{\varphi} = \varphi\mathrm{d}t + \mathrm{d}X^\varphi$, and $\mathrm{d}\tilde{\Delta} = \Delta\mathrm{d}t + \mathrm{d}X^\Delta$, where $X^\eta = (X_t^\eta)_{t\geqslant 0}$, $\eta \in \{\Omega, \varphi, \Delta\}$. Because of the semiclassical atom-light interactions and high photon number, we treat the control noises X classically, as in Refs. [23,24].

It is important to note that the term $\frac{1}{2}S^\dagger S\mathrm{d}[X]_t$ in Eq. (2) is absent in stochastic Hamiltonian methods [35,36,49], where stochasticity is introduced by directly incorporating noise realizations into the Hamiltonian and subsequently solving the resultant Schrödinger equation. Although numerical normalization for stochastic Hamiltonian methods averts issues when $S^\dagger S = I$, discrepancies arise when $S^\dagger S \neq I$, thus necessitating the inclusion of the term $S^\dagger S$ to ensure physically accurate results.

In this work, we distinguish between three classes of noise operators S,

$$\begin{aligned}
\text{Pauli noise:}\quad & [H, S] = 0, \quad S^\dagger S = I \\
& (\text{e.g., } S = \sigma_X, \sigma_Y, \sigma_Z), \\
\text{Projection noise:}\quad & [H, S] = 0, \quad S^\dagger S = S \\
& (\text{e.g., } S = (I - \sigma_Z)/2). \\
\text{Noncommuting:}\quad & H = \alpha\sigma_1, \quad S = \sigma_2, \\
& [H, S] = 2i\alpha\sigma_3,
\end{aligned}$$

Hence, Pauli noise would model noise in the control intensity (or phase via a formal expansion of the exponential function), whereas projection noise captures variations in control frequency. In scenarios involving noncommuting operators, any cyclic permutation within the set $\{\sigma_X, \sigma_Y, \sigma_Z\}$ can be used to model noise instances where the noise strengths in detuning and Rabi frequency exhibit comparable magnitudes.

For our simulation results, we consider the following three examples of noise processes.

1. White noise WN process

Here X takes the form

$$X_t = \gamma\int_0^t \mathrm{d}W_s, \quad \gamma \geqslant 0,$$

where $W = (W_t)_{t\geqslant 0}$ is a standard Brownian motion with quadratic variation $[X]_t = \gamma\,\mathrm{d}t$. The corresponding SSE reads

$$\mathrm{d}\psi = -iH\psi\,\mathrm{d}t - \tfrac{1}{2}\gamma^2 S^\dagger S\psi\,\mathrm{d}t - i\gamma S\psi\,\mathrm{d}W_t. \tag{3}$$

Using (3) to deduce the evolution of the state $\psi\psi^\dagger$ and taking the expectation results in the Lindblad equation for the density matrix $\rho = \mathbb{E}[\psi\psi^\dagger]$ [7,50] (see Appendix A)

$$\partial_t\rho = -i[H, \rho] + S\rho S^\dagger - \tfrac{1}{2}\{S^\dagger S, \rho\},$$

thus providing a valid unraveling of this master equation.

2. Ornstein-Uhlenbeck OU process

For a fixed constant $k > 0$, the OU process is given by

$$\mathrm{d}X_t = -kX_t\,\mathrm{d}t + \gamma\,\mathrm{d}W_t,$$

subjected to either the calibrated initial data, $X_0 = 0$, or distributed according to the stationary distribution of the OU process, i.e., $X_0 \sim \gamma\mathcal{N}/\sqrt{2k}$, where $\mathcal{N}$ is the standard normal distribution. The OU process can be seen as a damped WN process, in line with the fluctuation-dissipation relation. In contrast, WN is a limiting case of OU with $k \downarrow 0$ (taking the

limit of $k \to 0$ with $k > 0$) [51]. OU processes resemble $1/f$ noise in the high-frequency domain due to their power spectral density [52,53] and have been found to describe noise in an exceptionally broad range of physical processes [48,54]. The SSE with OU noise reads

$$\mathrm{d}\psi = -iH\psi\,\mathrm{d}t - \tfrac{1}{2}\gamma^2 S^\dagger S\psi\,\mathrm{d}t - iS\psi\,\mathrm{d}X_t. \tag{4}$$

Note that it has the same quadratic variation as WN.

3. Feedback (FB) process

If X_t is a semimartingale, then so are all processes of the form

$$\mathrm{d}Y_t = \begin{cases} \mathrm{d}X_t & \text{for } t < \tau, \\ \mathrm{d}X_t - \mu_P\,\mathrm{d}X_{t-\tau} - \mu_I X_{t-\tau}\,\mathrm{d}t & \text{for } t \geqslant \tau, \end{cases} \tag{5}$$

where $\tau > 0$ is a delay time and $\mu_I, \mu_P \in \mathbb{R}$. Here the quadratic variation of $Y = (Y_t)_{t\geqslant 0}$ satisfies

$$\mathrm{d}[Y]_t = \left(1 + \mu_p^2 \mathbb{1}(t > \tau)\right)\mathrm{d}[X]_t.$$

The FB process can be seen as a delayed proportional-integral (PI) controller applied to the noise [55], making it a viable noise mitigation technique that can be effectively analyzed using the SSE. In practice, this can be implemented by reading and processing control noise in real-time during state preparation, leading to the delay time τ [56]. Note that this list of noise processes is not exhaustive for the allowed colored noise processes in SSE. For instance, Brownian noise as integrated white noise or noise generated from arbitrary power spectral densities would pose interesting examples.

B. Analytical methods

Here we detail the methods used to derive the fidelity distribution for qubit systems evolving according to the SSE. Since the numerical integration of the SSE for ψ can be computationally expensive and unstable due to the non-Euclidean state space of the qubit and the possible nonlinearity introduced by the noise process, we derive full distribution solutions. These solutions yield explicit formulas for both the expectation and variance of the fidelity, offering precise results for individual noise manifestations instead of mean behavior approximations or bounds.

1. System of SDEs

The quantity of interest in quantum computing is the fidelity $\mathsf{F} := |\phi^\dagger\psi|^2$, where ϕ is the desired state without noise, i.e., ϕ satisfies the Schrödinger equation (1) and ψ evolves according to Eq. (2) [33].

To derive an explicit formula for F, we recursively derive a system of real-valued SDEs for a vector $\mathsf{V} \in \mathbb{R}^m$, $m \in \mathbb{N}$, taking the form

$$\mathrm{d}\mathsf{V} = A\mathsf{V}\,\mathrm{d}t + B\mathsf{V}\,\mathrm{d}X_t + a\,\mathrm{d}t + b\,\mathrm{d}X_t, \tag{6}$$

where the first component of V is the fidelity $\mathsf{F} = |\phi^\dagger\psi|^2$. The size of the system varies depending on the properties of the noise operator S. In the case of Pauli and projection noise on single qubits, $m = 3$, while in the noncommuting case, $m = 10$.

For WN, solving these equations involves considering $\mathsf{Y} = \mathbb{E}[\mathsf{V}]$ and solving the deterministic equation $\mathrm{d}\mathsf{Y} = A\mathsf{Y}\,\mathrm{d}t + a\,\mathrm{d}t$, which aligns with the Lindbladian approach (see Appendix A). However, for general noise, this approach is no longer applicable because $\mathbb{E}[\mathsf{V}\,\mathrm{d}X_t] \neq \mathbb{E}[\mathsf{V}]\mathbb{E}[\mathrm{d}X_t]$. Specifically for OU, terms such as $\mathbb{E}[X^2\mathsf{V}]$ arise. A common way to obtain a solution, as demonstrated in Ref. [57], is to extend the vector V with new entries of the form $X^{2n}\mathsf{V}$ and to derive an elaborate system that will then include $\mathbb{E}[X^{2n+1}\mathsf{V}]$. Eventually, an approximation has to be made to maintain a finite system. In Appendix B, we elaborate on the approximation $\mathbb{E}[X^{2n}\mathsf{V}] = \mathbb{E}[X^{2n}]\mathbb{E}[\mathsf{V}]$. The truncation point n, referred to as the *approximation order*, is the point at which an analytical solution for $\mathbb{E}[\mathsf{V}]$ can be found. As shown in Sec. II C 1, solutions improve with increasing approximation order but eventually become nonphysical as fidelities exceed the interval [0,1].

Instead, we advocate the less intuitive approach of deriving the full distribution of V, from which the expectation and higher-order moments can be inferred. In all cases explored in this work—except for the noncommuting case—we obtain a diagonalizable system (12), giving

$$\mathrm{d}\mathsf{Z} = \left(-\tfrac{1}{2}\gamma^2\Lambda^\dagger\Lambda\,\mathrm{d}t + \Lambda\,\mathrm{d}X_t\right)(\mathsf{Z} - c),$$

where $\{\Lambda, P\}$ is the eigensystem for both A and B, $\mathsf{Z} := P^{-1}\mathsf{V}$, and c is a vector of constants depending only on a and b. Using Ito's formula [39], the solution of this SDE is given by

$$\mathsf{Z} = \exp(\Lambda(X_t - X_0))(\mathsf{Z}_0 - c) + c,$$

thus yielding,

$$\mathsf{V} = P(\exp(\Lambda(X_t - X_0))(\mathsf{Z}_0 - c) + c),$$

from which an expression for the fidelity F can be derived.

2. Pauli noise

For Pauli noise, the SDE system (6) for the vector

$$\mathsf{V} = \begin{bmatrix} \mathsf{F} \\ |\phi^\dagger S\psi|^2 \\ i(\phi^\dagger S\psi\psi^\dagger\phi - \phi^\dagger S\psi\psi^\dagger\phi) \end{bmatrix} \in \mathbb{R}^3,$$

is given by $a = b = 0$,

$$A = \gamma^2\begin{bmatrix} -1 & 1 & 0 \\ 1 & -1 & 0 \\ 0 & 0 & -2 \end{bmatrix}, \quad B = \begin{bmatrix} 0 & 0 & -1 \\ 0 & 0 & 1 \\ 2 & -2 & 0 \end{bmatrix}.$$

Notice that $A = \gamma^2 B^2/2$. After applying the diagonalization method, we deduce the following expression for the fidelity:

$$\begin{aligned} \mathsf{F} &= \tfrac{1}{2}\left(1 + \mathsf{S}_0^2\right) + \tfrac{1}{2}\left(1 - \mathsf{S}_0^2\right)\cos(2(X_t - X_0)) \\ &= \cos^2(X_t - X_0) + \mathsf{S}_0^2\sin^2(X_t - X_0), \end{aligned} \tag{7}$$

where $\mathsf{S}_0 = \phi_0^\dagger S\phi_0$. For the WN and OU noise process, we deduce explicit formulas for the expectation and variance for the fidelity (cf. Appendix C).

a. OU process. For calibrated initial data (i.e., $X_0 = 0$), we find the explicit formulas

$$\begin{aligned} \mathbb{E}\left[\mathsf{F}_t^{\mathrm{OU}}\right] &= \tfrac{1}{2}\left(1 + \mathsf{S}_0^2\right) + \tfrac{1}{2}\left(1 - \mathsf{S}_0^2\right)e^{-2\gamma^2\tau_k(t)}, \\ \mathrm{Var}\left(\mathsf{F}_t^{\mathrm{OU}}\right) &= \tfrac{1}{8}\left(1 - \mathsf{S}_0^2\right)^2[1 - e^{-4\gamma^2\tau_k(t)}]^2, \end{aligned} \tag{8}$$

with $\tau_k(t) := e^{-kt}\sinh(kt)/k$, while for stationary initial data (i.e., $X_0 \sim \gamma\mathcal{N}/\sqrt{2k}$), we obtain

$$\mathbb{E}\big[\mathsf{F}_t^{\mathrm{OU}}\big] = \tfrac{1}{2}\big(1+\mathsf{S}_0^2\big) + \tfrac{1}{2}\big(1-\mathsf{S}_0^2\big)e^{-2(1-e^{-kt})\frac{\gamma^2}{k}},$$
$$\mathrm{Var}\big(\mathsf{F}_t^{\mathrm{OU}}\big) = \tfrac{1}{8}\big(1-\mathsf{S}_0^2\big)^2[1-e^{-4(1-e^{-kt})\frac{\gamma^2}{k}}]^2.$$

b. WN process. Passing $k \downarrow 0$ in (8) and using the fact that $\lim_{k\downarrow 0}\tau_k(t) = t$, we recover the expectation and variance for the WN case:

$$\mathbb{E}\big[\mathsf{F}_t^{\mathrm{WN}}\big] = \tfrac{1}{2}\big(1+\mathsf{S}_0^2\big) + \tfrac{1}{2}\big(1-\mathsf{S}_0^2\big)e^{-2\gamma^2 t},$$
$$\mathrm{Var}\big(\mathsf{F}_t^{\mathrm{WN}}\big) = \tfrac{1}{8}\big(1-\mathsf{S}_0^2\big)^2[1-e^{-4\gamma^2 t}]^2.$$

Notice the difference between the large-time asymptotic fidelity values for the WN and OU processes:

$$\lim_{t\to\infty}\mathbb{E}\big[\mathsf{F}_t^{\mathrm{OU}}\big] = \tfrac{1}{2}\big(1+\mathsf{S}_0^2\big) + \tfrac{1}{2}\big(1-\mathsf{S}_0^2\big)e^{-\frac{\gamma^2}{k}} \geqslant \tfrac{1}{2}\big(1+\mathsf{S}_0^2\big) = \lim_{t\to\infty}\mathbb{E}\big[\mathsf{F}_t^{\mathrm{WN}}\big],$$

and

$$\lim_{t\to\infty}\mathrm{Var}\big[\mathsf{F}_t^{\mathrm{OU}}\big] \leqslant \lim_{t\to\infty}\mathrm{Var}\big[\mathsf{F}_t^{\mathrm{WN}}\big],$$

indicating a better large-time asymptotic fidelity for the OU process, which is logical given that OU noise is inherently damped.

3. Projection noise

Next, we consider projection noise. For the vector

$$\mathsf{V} = \begin{bmatrix} \mathsf{F} \\ \phi^\dagger S\psi\psi^\dagger\phi + \phi^\dagger\psi\psi^\dagger S\phi \\ i(\phi^\dagger S\psi\psi^\dagger\phi - \phi^\dagger S\psi\psi^\dagger\phi) \end{bmatrix} \in \mathbb{R}^3,$$

we find the SDE system (6) with

$$A = -\frac{\gamma^2}{2}\begin{bmatrix}0&1&0\\0&1&0\\0&0&1\end{bmatrix}, \quad B = \begin{bmatrix}0&0&1\\0&0&1\\0&1&0\end{bmatrix},$$
$$a = \gamma^2\mathsf{S}_0^2\begin{bmatrix}1\\1\\0\end{bmatrix}, \quad b = \mathsf{S}_0^2\begin{bmatrix}0\\0\\-2\end{bmatrix}.$$

The diagonalization method then gives the fidelity

$$\mathsf{F} = 1 - 2\big(1-\mathsf{S}_0^2\big)\mathsf{S}_0^2(1-\cos(X_t - X_0)). \tag{9}$$

As in the previous case, explicit formulas for the expectation and variance for fidelity can be deduced under WN and OU noise processes (cf. Appendix C).

4. Noncommuting

For the noncommuting scenario, a closed SDE system of size $m = 10$ can be derived due to the group structure of the Pauli matrices. Here we find a system where the matrix A decomposes as $A = \alpha A_c + \gamma^2 B^2/2$, such that

$$\mathrm{d}\mathsf{V} = \alpha A_c\mathsf{V}\,\mathrm{d}t + \frac{\gamma^2}{2}B^2\mathsf{V}\,\mathrm{d}t + B\mathsf{V}\,\mathrm{d}X_t,$$

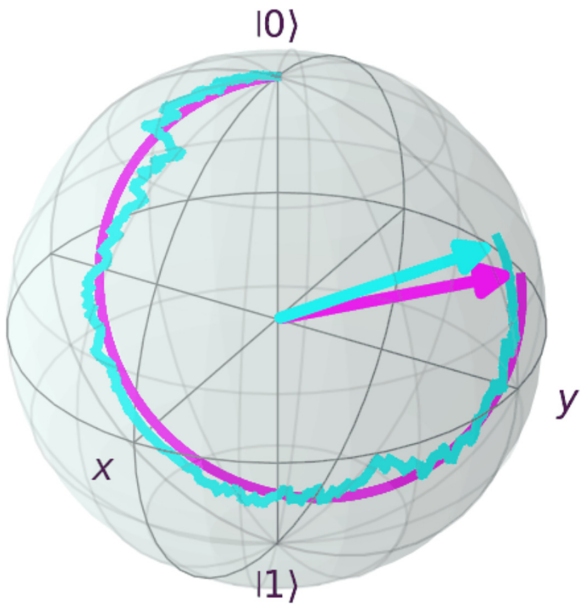

FIG. 2. Illustration of state trajectories on the Bloch sphere with $H = X + Z$ without noise (pink), and with Pauli OU noise with $S = X$, $k = 0.1$, $\gamma = 0.2$ (cyan).

where A_c represent the commutator terms and B^2 denotes the noise terms (see Appendix G for full matrices). In the absence of A_c, the system can be solved using the diagonalization method outlined in Sec. II B 1. However, the noncommutativity between A_c and B presents a hurdle for the full system. In such cases, presuming the dominance of the driving Hamiltonian over noise intensity, i.e., $\gamma^2/\alpha \ll 1$ (high signal-to-noise ratio), an approximation for the fidelity can be obtained using the stochastic Magnus expansion [58] (see Appendix G).

a. WN process. For the white noise case, an approximation is given by

$$\mathbb{E}[\mathsf{F}] \approx \tfrac{1}{2} + \tfrac{1}{2}\mathsf{C}_1^2 e^{-2\gamma^2 t} + \tfrac{1}{2}e^{-\gamma^2 t}\big(\sinh(u)\big(\big(\mathsf{C}_2^2 - \mathsf{C}_3^2\big)\cos(2at) - 2\mathsf{C}_2\mathsf{C}_3\sin(2at)\big) + \big(\mathsf{C}_2^2 + \mathsf{C}_3^2\big)\cosh(u)\big), \tag{10}$$

where $\mathsf{C}_i = \phi_0^\dagger\sigma_i\phi_0$ with $\mathsf{C}_1^2 + \mathsf{C}_2^2 + \mathsf{C}_3^2 = 1$ and $u = \gamma^2\sin(2\alpha t)/2\alpha$. This expression reveals the oscillatory behavior induced by the Hamiltonian. This can be explained by considering $H = X, S = Y$ and $\psi_0 = |0\rangle$ (see Fig. 2). Initially, the state is affected by the $S = Y$ noise. As evolution under H progresses, the state transitions to $(|0\rangle + |1\rangle)/\sqrt{2}$, which, as an eigenstate of S, is immune to this noise. Subsequently, it transitions to $|1\rangle$, once again becoming susceptible. This cyclic process results in the observed oscillations, with the frequency contingent upon the strength of the Hamiltonian α.

b. OU process. Unfortunately, we were unable to derive a satisfactory approximation of the fidelity expectation with the OU noise process. Nevertheless, we offer a rudimentary approximation for a certain parameter range in Appendix G. Moreover, our approach allows for a rapid and stable numerical solution of the SDE system to be obtained.

5. Multiqubit

In work by Kobayashi and Yamamoto [33], noise acting on multiple qubits is analyzed for multiqubit operators satisfying $S^\dagger S = I$. These are important cases, as noise on the $S = Z \otimes Z$ operator could model noise during an entanglement procedure, while $S = X \otimes I$ or $S = I \otimes X$ represents noise acting on one of the qubits in the system. However, Ref. [33] emphasizes that operators of the form $I \otimes Q + Q \otimes I$, with $Q^2 = I$, cannot be treated with their methods. These types of operators are also important cases, as they model noise on a global control that addresses all qubits simultaneously, which is prevalent in many quantum computing systems [59].

With our methods, we can solve these systems by defining $R := Q \otimes Q$, such that

$$S^\dagger S = I \otimes Q^2 + Q^2 \otimes I + 2R.$$

For Pauli noise ($Q^2 = I$), we obtain

$$\mathsf{F} = \tfrac{1}{4}\big(\mathsf{S}_0^2 + (\mathsf{R}_0 - 1)^2 + 2\big(1 - \mathsf{R}_0^2\big)\cos(2(X_t - X_0)) + (1 - \mathsf{S}_0 + \mathsf{R}_0)(1 + \mathsf{S}_0 + \mathsf{R}_0)\cos^2(2(X_t - X_0))\big), \tag{11}$$

with $\mathsf{S}_0 = \phi_0^\dagger S \phi_0$ and $\mathsf{R}_0 = \phi_0^\dagger R \phi_0$.

For projection noise ($Q^2 = Q$), we find

$$\mathsf{F} = 1 - 2(\cos(X_t - X_0) - 1) \times \big(\mathsf{S}_0^2 + \mathsf{S}_0(2\mathsf{R}_0(\cos(X_t - X_0) - 1) - 1) - 2\mathsf{R}_0[\mathsf{R}_0(\cos(X_t - X_0) - 1) + \cos(X_t - X_0)]\big).$$

If we assume that the two-qubit system starts in a product state $\phi_0 = \phi_0^{(0)} \otimes \phi_0^{(1)}$, then the values S_0 and R_0 can be expressed as $\mathsf{S}_0 = \mathsf{S}_0^{(0)} + \mathsf{S}_0^{(1)}$ and $\mathsf{R}_0 = \mathsf{S}_0^{(0)}\mathsf{S}_0^{(1)}$, where the superscript (i) refers to the ith qubit. For both Pauli and projection noise, the fidelity distribution then factors as

$$\mathsf{F} = \mathsf{F}^{(0)}\mathsf{F}^{(1)}. \tag{12}$$

This result aligns with physical intuition: Although the two qubits evolve independently, they are subjected to the same noise process. Hence, their fidelities depend solely on the noise, leading to a factorization at the distribution level. Yet, this does not imply independence of the expectations $\mathbb{E}[\mathsf{F}^{(0)}]$ and $\mathbb{E}[\mathsf{F}^{(1)}]$. The full expectation $\mathbb{E}[\mathsf{F}]$ can still be determined using the methods of Appendix C. Furthermore, the two-qubit method can accommodate entangled ground states for which the distributions deviate from the factorized form depicted in (12). In Appendix D, we extend this analysis to N-qubit systems.

6. Feedback process

Combining (5) and (7) for Pauli noise [or similarly (9) for projection noise], we obtain the fidelity for an FB process with OU as the base noise (see Appendix C). The resulting expression is given by

$$\mathbb{E}[\mathsf{F}] = \frac{1}{2}\big(1 + S_0^2\big) + \frac{1}{2}\big(1 - S_0^2\big)\mathbb{E}[\cos(2(Y_t - Y_0))] = \exp\Big(- \frac{\gamma^2}{k}(1 - e^{-2kt}) - \alpha\frac{2\gamma^2}{k}e^{-k\tau}(1 - e^{-2k(t-\tau)}) - \alpha^2\frac{\gamma^2}{k}(1 - e^{-2k(t-\tau)}) - \alpha\beta\frac{4\gamma}{k}(1 - e^{-k(t-\tau)}) - \beta\frac{4\gamma}{k}e^{-k\tau}(1 - e^{-k(t-\tau)}) - \beta^2 2(t - \tau)\Big), \tag{13}$$

where $\alpha = -(\mu_P k - \mu_I)/k$ and $\beta = (\mu_P k - \mu_I)\gamma/k - \mu_P$.

Differentiating this expression allows us to find the optimal values of the PI controller constants as $\mu_P = \exp(-k\tau)$ and $\mu_I = 0$. This demonstrates the applicability of our method in analyzing the impact of various feedback and error mitigation processes on qubit fidelity.

C. Simulation results

In this section, we validate our fidelity calculations by comparing them with Monte Carlo simulations. Throughout, we employ the explicit second-order scheme due to Platen [60,61] as our Monte Carlo stochastic integration method, outlined in Appendix E. We also set the driving Hamiltonian $H = 0$ without loss of generality as $[H, S] = 0$, unless explicitly stated otherwise. In the context of current-era quantum computers, a signal-to-noise ratio $\gamma^2/\alpha \approx 0.01$ is realistic Refs. [2,62,63]. Consequently, we choose the values of γ, k, and α accordingly in all cases. We also refer the reader to the time-rescaling argument discussed in Appendix G.

1. Pauli noise and truncation

We start by showing that the approximation order, as detailed in Sec. II B 1, becomes better with increasing order but eventually leads to nonphysical behavior. For the Pauli noise system, we get an evolution for the vector $\boldsymbol{x} = \mathbb{E}[\mathsf{V}]$ given by

$$\dot{\boldsymbol{x}} = \begin{bmatrix} -\gamma^2 & \gamma^2 & ik \\ \gamma^2 & -\gamma^2 & -ik \\ 2ip & -2ip & -k - 2\gamma^2 \end{bmatrix}\boldsymbol{x}, \quad \boldsymbol{x}(0) = \begin{bmatrix} 1 \\ \mathsf{S}_0^2 \\ 0 \end{bmatrix},$$

with $p = (k\mathbb{E}[X_t^2] - \gamma^2)$ and $\mathsf{S}_0 = |\phi_0^\dagger S \phi_0|$. Here we made the assumption $\mathbb{E}[X_t^2\mathsf{V}] = \mathbb{E}[X_t^2]\mathbb{E}[\mathsf{V}]$ to close the system.

The second-order system is detailed in Appendix F. Using the fact that $\mathbb{E}[X_t^2] = (1 - e^{-2kt})\gamma^2/2k$ (see Appendix C), we can solve these systems numerically [64].

From Fig. 3, we see that the truncation approach performs well for high fidelities. Notably, the second-order solution follows the exact solution longer than the first-order does. This shows that the Itô isometry [65] approximation of Appendix B works relatively well for short durations. However, both orders eventually lead to nonphysical behavior, as fidelities are predicted beyond the interval [0,1] and thus fail to correctly predict long-time behavior. This issue becomes particularly critical when considering optimal control methods for the SSE, where the stability of the fidelity must be maintained over extended periods. This underscores the significance of our full-distribution method, which accurately predicts the long-time fidelity behavior. In Fig. 4, we see the convergence of the sample mean towards the analytic mean when increasing the number of trials. As in Fig. 3, we use a low number of trials to maintain a visible difference between the sample mean and the analytic mean for the other experiments.

In Fig. 5, we present the full fidelity distributions over time. The histograms depict fidelities derived from 2×10^3

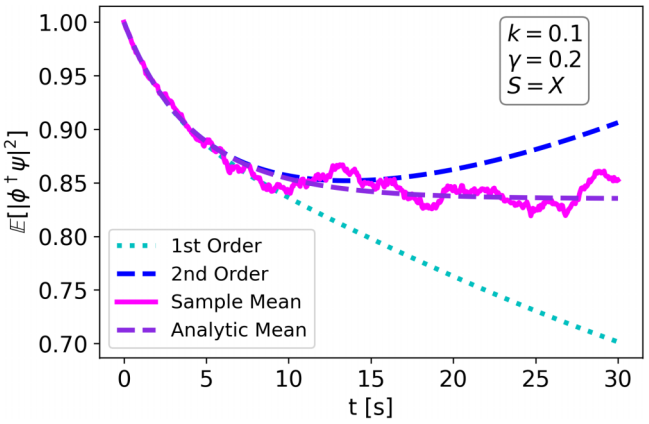

FIG. 3. Pauli noise: Fidelity expectations for a 1 qubit system with $S = X$, $\gamma = 0.2$, $k = 0.1$ and calibrated initial data. First and second order of approximation together with sample mean and analytic mean as in Eq. (8). Computed with 2×10^2 Monte-Carlo simulations.

Monte Carlo SSE samples (requiring approximately 30 min on an eight-core laptop). In contrast, we determine the kernel density estimate [66] of 1×10^3 OU noise realizations (taking mere seconds on the same setup), resulting in the solid distribution lines. This comparison highlights the accuracy of our distribution method while significantly reducing computational overhead. Moreover, Fig. 5 shows that the distributions maintain their shape over time, with their peaks swiftly shifting towards zero fidelity.

2. Projection noise

For the projection noise, we take $S = |1\rangle\langle 1|$ and analyze the fidelity for both the OU and the WN noise. As depicted in Fig. 6, initially, OU noise and WN noise exhibit similar fidelity behaviors but quickly diverge, leading to differing large-time asymptotic values. This discrepancy is expected due to the distinct characteristics of the noise processes: While the second moment of WN grows as $\mathbb{E}[X_t^2] = \gamma^2 t$, for OU noise, $\lim_{t\to\infty} \mathbb{E}[X_t^2] = \gamma^2/2k$. Hence, the WN process drifts

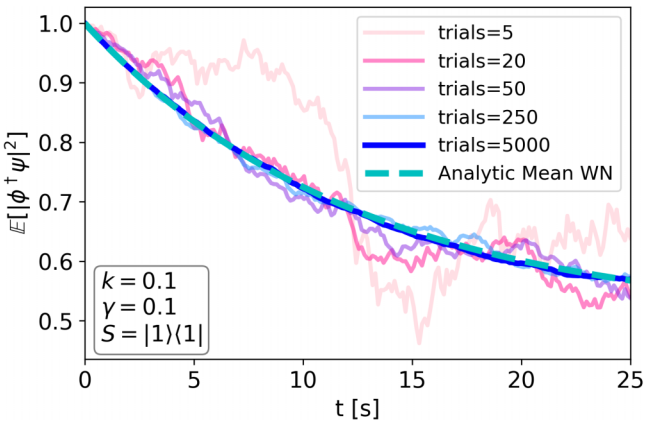

FIG. 4. Projection noise: Convergence plot for different number of trials compared to analytic mean. 1 qubit system with $S = |1\rangle\langle 1|$, $\gamma = 0.1$, $k = 0.1$ and stationary initial data, with analytic mean.

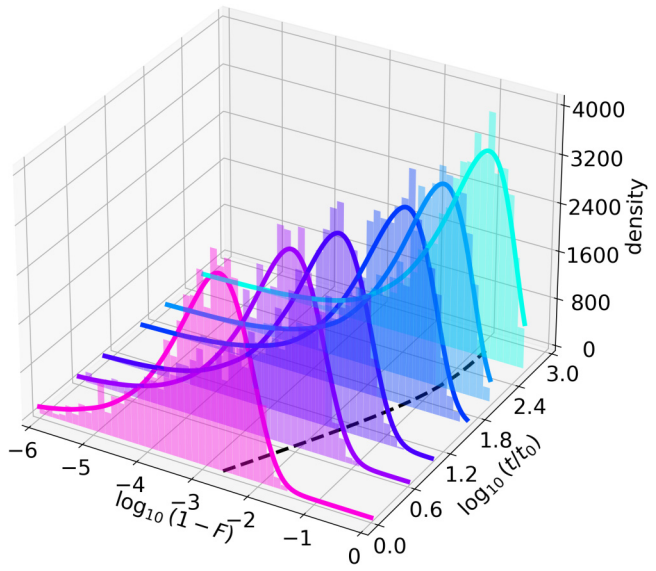

FIG. 5. Pauli noise: Fidelity distributions at various times t for a one-qubit system with $S = X$, $\gamma = 0.2$, $k = 0.1$ and calibrated initial data as in (7). Solid lines are kernel density estimates of distributions as in (7) and histograms are from Monte Carlo samples of (4). Here $t_0 = 0.06$ is a fixed reference timescale. Fidelity expectations are depicted in dashed black line; 2×10^3 Monte Carlo simulations for each curve and histogram.

away over time while the OU noise continues to fluctuate around zero, constantly self-correcting. This behavior is also evident in Fig. 6, where the variance of the fidelity under WN noise grows significantly faster than under OU noise, as indicated by the shaded area.

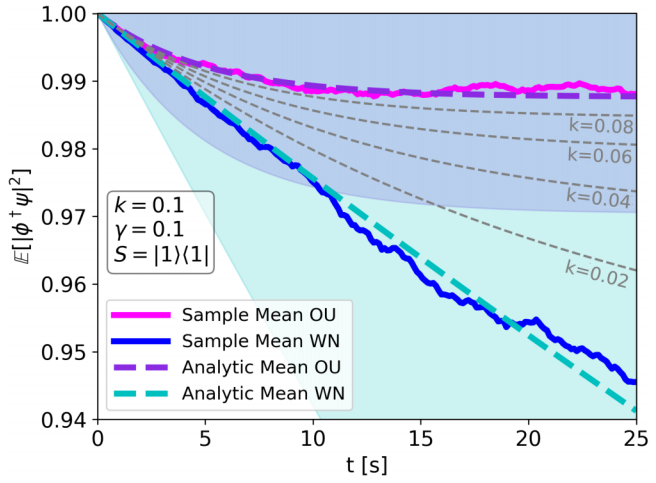

FIG. 6. Projection noise: Fidelity expectations and standard deviations (shaded areas) for a 1-qubit system with $S = |1\rangle\langle 1|$, $\gamma = 0.1$, $k = 0.1$ (and $k = 0$ for WN) and stationary initial data, with sample mean, analytic mean, and analytic variances. The transition from WN to OU is indicated by gray dashed lines signifying equivalent cases with $k = 0.02, 0.04, 0.06, 0.08$. Computed with 5×10^2 Monte Carlo samples.

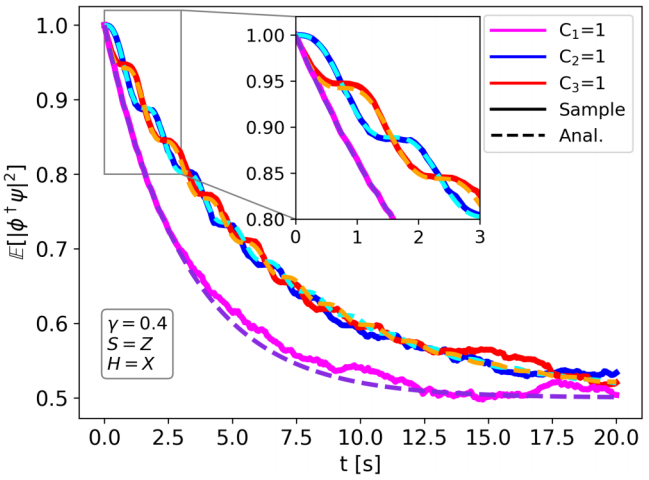

FIG. 7. Noncommuting: Fidelity expectations for a 1-qubit system with $S = Z$, $H = X$, $\gamma = 0.4$, and calibrated initial data. Sample mean and analytic mean as in (10) with varying conditions for $C_1^2 + C_2^2 + C_3^2 = 1$. Computed with 1×10^3 Monte Carlo samples.

3. Noncommuting

We analyze the noncommuting case outlined in Sec. II B 4. From Fig. 7, we see that the sample mean fidelities align closely with the predictions derived in (10). These fidelities indeed exhibit the expected oscillating behavior induced by the noncommuting Hamiltonian, cycling through areas where the state is susceptible to noise. The agreement with Monte Carlo simulations for long-time behavior can be attributed to the stochastic Magnus expansion-type approximation.

Furthermore, when $C_1 = 1$, signifying the initial state as an eigenstate of the Hamiltonian, the fidelity decreases exponentially with a rate $-2\gamma^2$ since it does not cycle in and out of the noise susceptibility region. On the other hand, for $C_2 = 1$ or $C_3 = 1$, the state oscillates between susceptibility and immunity to noise, leading to a slower exponential decrease in fidelity with an average rate of $-\gamma^2$, half of the previous scenario. Also note the distinction between $C_2 = 1$ and $C_3 = 1$ from the inset of Fig. 7: While $C_2 = 1$ corresponds to an initial state that is immune to noise—it is an eigenstate of the noise operator—$C_3 = 1$ renders it highly susceptible, causing an immediate fidelity drop, following the $C_1 = 1$ curve until the Hamiltonian's rotational effect sets in.

4. Multiqubit

Last, we investigate a two-qubit system subjected to the noise operator $S = X \otimes I + I \otimes X$. We examine both the product initial state $\phi_0 = |00\rangle$ (which could also be treated as the product of the distributions of the individual qubits, cf. Appendix D) and the maximally entangled $|\mathrm{GHZ}\rangle$ state [67] given by $\phi_0 = |\mathrm{GHZ}\rangle = (|00\rangle + |11\rangle)/\sqrt{2}$. As depicted in Fig. 8, our distribution method matches the Monte Carlo simulation results. Interestingly, we observe that both the coupling and the colored noise tend to favor higher fidelities, surpassing the value of 0.25, which would be the case for an uncoupled system. The ability of a coupled system to reach higher fidelities under colored noise, previously analyzed in Ref. [68], conforms to our observations.

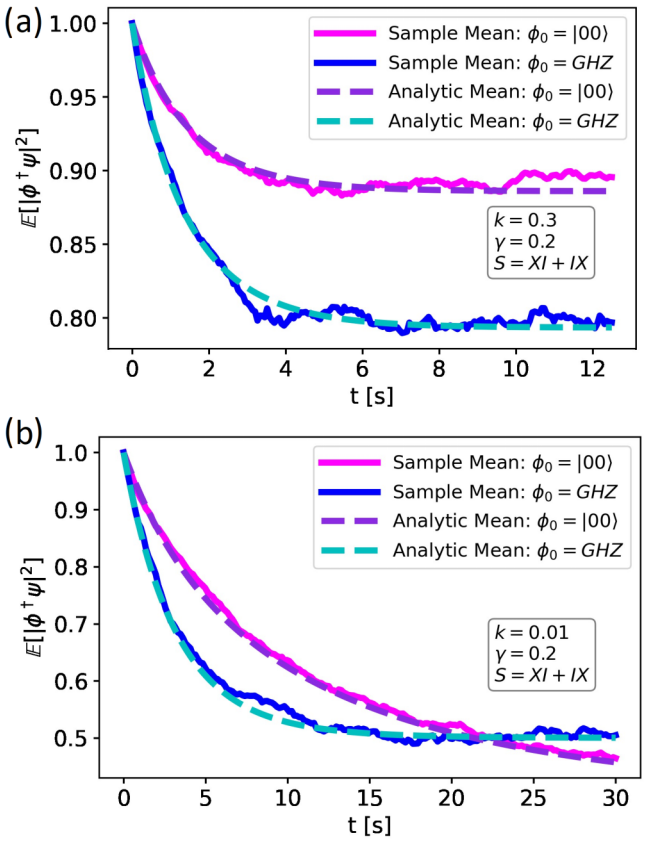

FIG. 8. Two-qubit: Fidelity expectations for a two-qubit system with $S = X \otimes I + I \otimes X$, $\gamma = 0.2$ and stationary initial data. (a) $k = 0.3$ and (b) $k = 0.01$. The sample and analytic means for $|00\rangle$ and $|\mathrm{GHZ}\rangle$ initial state, as calculated in (11). Computed with 500 Monte Carlo samples.

Furthermore, we observe different results for product initial state and the entangled $|\mathrm{GHZ}\rangle$ state. This behavior can be explained if we write the initial state in the eigenbasis of the noise operator S. For $k \gg 1$, the sensitivity to noise is predominantly determined by the eigenvalues corresponding to the eigenvector components of the initial state. For $k \ll 1$, the noise approaches a Haar random measure on the accessible state space, which is determined by the number of nonzero eigenvectors in the initial state.

5. Feedback process

We examine the FB processes based on the expression of the fidelity in (13). Figure 9 illustrates the remarkable agreement between analytical and Monte Carlo fidelities. We see that for a commuting noise operator with OU noise, employing a mitigation process involving a PI controller with $\mu_P = 1$ and $\mu_I = 0$ proves to be highly effective. This efficacy is consistent with the logical reasoning that both the drive and the noise propel the state in the same direction. Therefore, this specific FB process tries to restore the state to its original position, mitigating the effects of noise. A PI controller with $\mu_p = 0$ and $\mu_I = 0.25$ also mitigates the noise up to a certain duration but eventually leads to deteriorating fidelities.

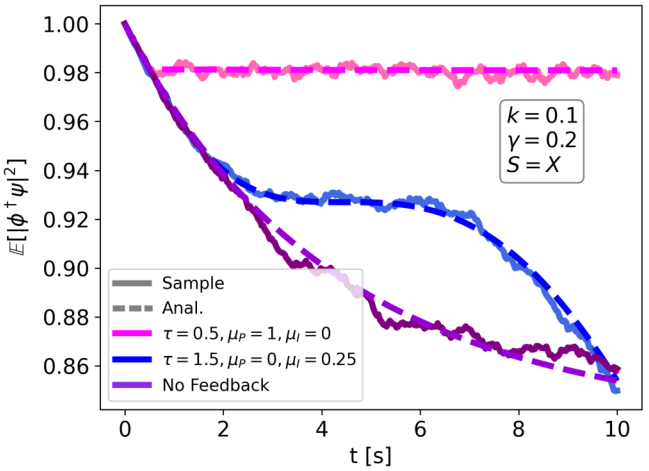

FIG. 9. Feedback process: Fidelity expectations for a one-qubit system with $S = X$, $\gamma = 0.2$, $k = 0.1$ and stationary initial data. The sample and analytic means for $|0\rangle$ initial state with different feedback parameters, as calculated in (13). Computed with 500 Monte Carlo samples.

III. DISCUSSION

This work presents a novel approach to characterize the full distribution of qubit fidelity under SSEs, offering richer insights compared to the traditional Lindblad equation. Our methodology not only aids in noise characterization but also holds promise for addressing optimal control challenges. Furthermore, our work predicts large-time fidelity behaviors for qubits evolving under realistic noise sources, such as OU noise stemming from fluctuation-dissipation processes. This large-time behavior is especially important in controlled processes, where one seeks to maintain a state faithfully for long periods. In addition, the computational efficiency and accuracy of our methods surpass conventional Monte Carlo techniques for SSEs, offering a compelling advantage. By accurately assessing noise levels in qubit control systems, such as those involving laser drivers or cavity resonators, our findings establish a robust benchmark for noise tolerance in such systems.

In future research, our aim is to broaden the scope of our investigations to include noises with arbitrary power spectral densities or even of a quantum nature. This will allow for a straightforward fidelity characterization of a quantum computing system based on measured noise profiles. Analysis on the power spectral densities might also allow for a characterization of the non-Markovianity of the noise, possibly leading to generic noise mitigation techniques. Furthermore, experimental validation of our models is imminent, with plans to introduce controlled noise signals for fidelity measurements, by introducing predefined exaggerated noise as a control signal to drown out existing signal noise. Fidelity distributions can then be measured through repeated measurements under the same noise realization. Last, we anticipate using SSEs for optimal noise mitigation in open quantum systems, a frontier that remains largely unexplored for master equations. Our envisioned contributions hold promise for advancing both theoretical understanding and practical applications in quantum computing and control.

ACKNOWLEDGMENTS

We thank Jasper Postema, Raul F. Santos, Madhav Mohan, and Jasper van de Kraats for fruitful discussions. This research is financially supported by the Dutch Ministry of Economic Affairs and Climate Policy (EZK), as part of the Quantum Delta NL program; the Horizon Europe programme HORIZON-CL4-2021-DIGITAL-EMERGING-01-30 via the project 101070144 — EuRyQa — HORIZON-CL4-2021-DIGITAL-EMERGING-01; and by the Netherlands Organisation for Scientific Research (NWO) under Grant No. 680.92.18.05. L.Y.V. and O.T. acknowledge support from NWO Grant No. NGF.1582.22.009.

R.J.P.T.d.K. proposed using SSE for noise analysis, performed the calculations, and carried out the numerical simulations. L.Y.V. contributed to the calculations on the SSE, in particular to the noncommuting cases. O.T. initiated the idea of using full distribution solutions and contributed to the theoretical analysis of the results. S.J.J.M.F.K. contributed to the quantum analysis of the model.

The authors declare no competing interests.

DATA AVAILABILITY

The data that support the findings of this article are openly available [69].

APPENDIX A: FORMAL DERIVATION OF THE STOCHASTIC SCHRÖDINGER EQUATION

One way of introducing noise into the Schrödinger equation, as described in Refs. [2,37], is to formally consider

$$\mathrm{d}\psi = -iH\psi\,\mathrm{d}X_t,$$

where X_t is a continuous noise profile. On the other hand, one expects the corresponding unitary propagator to take the form

$$U(t) = \exp\left(-iH(X_t - X_0)\right).$$

They indeed coincide whenever X_t is a cádlág adapted process with locally finite variation. However, this is not the case for general semimartingales like the Ornstein-Uhlenbeck and white noise processes. Indeed, applying Itô's formula to the unitary propagator yields

$$\mathrm{d}U(t) = -iHU(t)\,\mathrm{d}X_t - \tfrac{1}{2}H^2U(t)\,\mathrm{d}[X]_t,$$

which clearly deviates from the standard Schrödinger equation, thus motivating the stochastic Schrödinger equation.

In this section, we follow the derivation of the SSE as described in Ref. [28]. Consider an OU process X_t and operators C, D, and R on the Hilbert space. The standard Schrödinger equation with noise is given by

$$\mathrm{d}\psi = (C + DX_t)\psi\,\mathrm{d}t + R\psi\,\mathrm{d}X_t.$$

Using $\mathrm{d}X_t = -kX_t + \gamma\mathrm{d}W_t$, this can be rewritten as

$$\mathrm{d}\psi = (C + XD - kXR)\psi\,\mathrm{d}t + \gamma R\psi\,\mathrm{d}W_t.$$

For normalization, $\mathrm{d}|\psi|^2 = (\mathrm{d}\psi^\dagger)\psi + \psi^\dagger(\mathrm{d}\psi) + (\mathrm{d}\psi^\dagger)(\mathrm{d}\psi) = 0$ is required at all times. Expanding this using Ito

calculus ($\mathrm{d}t^2 = 0,\ \mathrm{d}W_t\mathrm{d}t = 0,\ \mathrm{d}W_t^2 = \mathrm{d}t$) [39] gives

$$\mathrm{d}|\psi|^2 = \psi^\dagger[C^\dagger + C + X_t(D^\dagger + D - kR - kR^\dagger) + \gamma^2 R^\dagger R]\psi\,\mathrm{d}t + \gamma\psi^\dagger(R^\dagger + R)\psi\,\mathrm{d}W_t = 0.$$

Thus, $C^\dagger + C + R^\dagger R = 0$, $D^\dagger + D - kR - kR^\dagger = 0$ and $R^\dagger + R = 0$. One can choose $R = iS$ with $S = S^\dagger$ Hermitian. Furthermore, $C = -iH - \frac{1}{2}S^\dagger S = -iH - \frac{1}{2}S^\dagger S$, with $H = H^\dagger$ and $D = 0$ to finally get the SSE for an OU process:

$$\mathrm{OU}: \quad \mathrm{d}\psi = -iH\psi\,\mathrm{d}t + ikX_tS\psi\,\mathrm{d}t - \frac{\gamma^2}{2}S^\dagger S\psi\,\mathrm{d}t - i\gamma S\psi\,\mathrm{d}W_t.$$

Letting $k \to 0$ results in the SSE for the WN process as

$$\mathrm{WN}: \quad \mathrm{d}\psi = -iH\psi\,\mathrm{d}t - \frac{\gamma^2}{2}S^\dagger S\psi\,\mathrm{d}t - i\gamma S\psi\,\mathrm{d}W_t.$$

Note that Ito calculus holds for any semimartingale [39] and, thus, for general semimartingale noise, we can write

$$\mathrm{SM}: \quad \mathrm{d}\psi = -iH\psi\,\mathrm{d}t - \tfrac{1}{2}S^\dagger S\psi\,\mathrm{d}[X]_t - iS\psi\,\mathrm{d}X_t,$$

where $[X]_t$ is the quadratic variation of the process [40]. If $S^\dagger S = I$, then the above equation exactly corresponds to a stochastic Hamiltonian approach where the result is normalized after every iteration step of the numerical scheme. However, if $S^\dagger S \neq I$, then only the SSE approach leads to the physically correct way of normalization. By defining $\rho = \mathbb{E}[\psi\psi^\dagger]$ and noting that $\mathbb{E}[\mathrm{d}W_t] = 0$

$$\begin{aligned}\mathrm{d}\psi\psi^\dagger &= -i[H, \psi\psi^\dagger]\,\mathrm{d}t + (S\psi\psi^\dagger S^\dagger - \tfrac{1}{2}\{S^\dagger S, \psi\psi^\dagger\})\,\mathrm{d}[X]_t - i[S, \psi\psi^\dagger]\,\mathrm{d}X_t\\ \Rightarrow \partial_t\rho &= -i[H, \rho] + \gamma^2(S\rho S^\dagger - \tfrac{1}{2}\{S^\dagger S, \rho\}) - i[S, \mathbb{E}[\psi\psi^\dagger\,\mathrm{d}X_t]],\end{aligned}$$

which for white noise reduces to the Lindblad equation since $\mathbb{E}[\psi\psi^\dagger\mathrm{d}X_t] = \mathbb{E}[\psi\psi^\dagger\mathrm{d}W_t] = \mathbb{E}[\psi\psi^\dagger]\mathbb{E}[\mathrm{d}W_t] = 0$. Note that for general noise, there is no independence of the state and the noise increments (i.e., $\mathbb{E}[\psi\psi^\dagger\mathrm{d}X_t] \neq \mathbb{E}[\mathrm{d}X_t]\rho$), and we do not get the standard Lindblad equation. It is, however, still possible to find an approximate closed-form non-Markovian master equation using the Nakajima-Zwanzig method [45].

APPENDIX B: APPROXIMATION USING ITO'S ISOMETRY

We detail the approximation method for terms of the form $\mathbb{E}[X_t^2\mathsf{V}]$ as described in Sec. II B 1. The integral solution of the OU process [70] can be written as

$$X_t = \int_0^t \gamma e^{k(s-t)}\mathrm{d}W_s.$$

By positivity of V

$$\mathbb{E}[X_t^2\mathsf{V}] = \mathbb{E}\left[\left(\int_0^t \gamma e^{k(s-t)}\mathrm{d}W_s\right)^2\mathsf{V}\right] = \mathbb{E}\left[\left(\int_0^t \gamma\sqrt{\mathsf{V}}e^{k(s-t)}\mathrm{d}W_s\right)^2\right].$$

If V were to be adapted to the natural filtration of the white noise process W_t, then Ito's isometry [65] can be used to write

$$\mathbb{E}[X_t^2\mathsf{V}] = \mathbb{E}\left[\int_0^t \gamma^2\mathsf{V}e^{2k(s-t)}\mathrm{d}t\right] = \frac{\gamma^2}{2k}(1 - e^{-2kt})\mathbb{E}[\mathsf{V}] = \mathbb{E}\big[X_t^2\big]\mathbb{E}[\mathsf{V}].$$

However, V could, for instance, be the fidelity at time t, which depends on the white noise process over the interval $[0, t]$. Therefore, Itô's isometry does not hold. Nevertheless, for small values of t, the values of V are roughly equal to their respective initial values, and Itô's isometry can be used as an approximation.

APPENDIX C: MOMENT CALCULATION

For the expectation and variance of the fidelity distributions, the expressions for the expectations of the terms $\cos(\alpha(X_t - X_0))$ for $\alpha > 0$ must be calculated [note that for the square terms $\cos(x)^2 = (\cos(2x) + 1)/2$]. To do so, the cosines are expanded into their power series representation, and both linearity and conditional expectations are used to get

$$\mathbb{E}[\cos(\alpha(X_t - X_0))] = \sum_{n=0}^{\infty}\frac{(-1)^n}{2n!}\alpha^{2n}\mathbb{E}[\mathbb{E}[(X_t - X_0)^{2n}|X_0]]. \tag{C1}$$

The OU process, by Ito's formula [65], can be shown to satisfy

$$\begin{aligned}\mathrm{d}X_t^n &= -nkX_t^n\mathrm{d}t + n\gamma X_t^{n-1}\mathrm{d}W_t + \tfrac{1}{2}(n^2 - n)\gamma^2X_t^{n-2}\mathrm{d}t, \qquad X^n(0) \sim X_0^n, \quad \forall n \in \mathbb{N}.\\ \mathrm{d}W_t^l &= lW_t^{l-1}\mathrm{d}W_t + \tfrac{1}{2}(l^2 - l)W_t^{l-2}\mathrm{d}t, \qquad W^l(0) \sim W_0^l, \quad \forall l \in \mathbb{N}.\end{aligned} \tag{C2}$$

1. Calibrated initial data $X_0 = 0$

For calibrated initial data (e.g., $X_0 = 0$), it is easily proven by induction that

$$\mathbb{E}[\mathbb{E}[(X_t - X_0)^{2n}|X_0]] = \mathbb{E}\big[X_t^{2n}\big] = \frac{\Gamma\left(n + \frac{1}{2}\right)}{\sqrt{\pi}}\left(\frac{2\gamma^2}{k}e^{-kt}\sinh(kt)\right)^n. \tag{C3}$$

where Γ is the gamma function. Resulting from Eq. (C1) in

$$\mathbb{E}[\cos(\alpha(X_t - X_0))] = \exp\left(-\alpha^2 \frac{\gamma^2}{2k} e^{-kt} \sinh(kt)\right).$$

2. Stationary initial data $X_0 \sim \gamma\mathcal{N}/\sqrt{2k}$

For stationary initial data, a slightly more involved approach is necessary. Employing the binomial theorem, one obtains

$$\mathbb{E}[(X_t - X_0)^{2n}|X_0] = \sum_{m=0}^{2n} \binom{2n}{m} (-1)^{2n-m} X_0^{2n-m} \mathbb{E}\left[X_t^m \middle| X_0\right]. \tag{C4}$$

From the differential equations in Eq. (C2)

$$\mathrm{d}\mathbb{E}\left[X_t^m \middle| X_0\right] = -mk\mathbb{E}\left[X_t^m|X_0\right]\mathrm{d}t + \tfrac{1}{2}(m^2 - m)\gamma^2 \mathbb{E}\left[X_t^{m-2}\middle|X_0\right]\mathrm{d}t,$$

with initial conditions $\mathbb{E}[X_t^0|X_0] = 1$, $\mathbb{E}[X_t^1|X_0] = X_0 e^{-kt}$. This can be shown to have the solution

$$\mathbb{E}\left[X_t^m \middle| X_0\right] = \begin{cases} e^{-2wkt}(2k)^{-w} \displaystyle\sum_{l=0}^{w} a[l, w](e^{2kt} - 1)^{w-l} \gamma^{2(w-l)} k^l X_0^{2l} & \text{with } w = \dfrac{m}{2} \text{ for } m \text{ even}, \\ e^{-(2w+1)kt}(2k)^{-w} \displaystyle\sum_{l=0}^{w} b[l, w](e^{2kt} - 1)^{w-l} \gamma^{2(w-l)} k^l X_0^{2l+1} & \text{with } w = \dfrac{m-1}{2} \text{ for } m \text{ odd}, \end{cases} \tag{C5}$$

with the coefficients

$$a[l, w] := 2^l \prod_{q=l+1}^{w} \frac{q(2q-1)}{q-l}, \qquad b[l, w] := 2^l \prod_{q=l}^{w-1} \frac{(1+q)(3+2q)}{(q-l+1)}.$$

For verification, the expressions for $\mathbb{E}[X_t^{2m}]$ in the case of calibrated initial data [Eq. (C3)] are retrieved when taking $X_0 = 0$. Using conditional expectation on Eq. (C4) gives

$$\mathbb{E}[\mathbb{E}[(X_t - X_0)^{2n}|X_0]] = \sum_{m=0}^{2n} \binom{2n}{m} (-1)^{2n-m} \mathbb{E}\left[X_0^{2n-m} \mathbb{E}\left[X_t^m \middle| X_0\right]\right]. \tag{C6}$$

Furthermore, the normal distribution of X_0 gives

$$\mathbb{E}\left[X_0^q\right] = \begin{cases} \left(\frac{\gamma}{\sqrt{2k}}\right)^q (q-1)!!, & q \text{ even} \\ 0, & q \text{ odd}. \end{cases} \tag{C7}$$

Combining Eq. (C5) and Eq. (C7), and filling into Eq. (C6) gives

$$\mathbb{E}[\mathbb{E}[(X_t - X_0)^{2n}|X_0]] = (2n-1)!! \left(\frac{\gamma^2}{k} e^{-kt}(e^{kt} - 1)\right)^n,$$

which, when used in Eq. (C1), results in

$$\mathbb{E}[\cos(\alpha(X_t - X_0))] = \exp\left(-\alpha^2 \frac{\gamma^2}{2k} e^{-kt}(e^{kt} - 1)\right).$$

3. Feedback process

We assume a semimartingale feedback process Y_t as

$$dY_t = \begin{cases} dX_t, & t < t^*, \\ dX_t - \mu_P dX_{t-t^*} - \mu_I X_{t-t^*} dt, & t \geqslant t^* \end{cases},$$

and want to determine $\mathbb{E}[\cos(Y_t - Y_0)]$. For OU noise, we can rewrite this as

$$dY_t = \begin{cases} dX_t, & t < t^*, \\ dX_t - \alpha dX_{t-t^*} - \beta dW_{t-t^*}, & t \geqslant t^* \end{cases},$$

with $\alpha = -(\mu_P k - \mu_I)/k$ and $\beta = (\mu_P k - \mu_I)\gamma/k - \mu_P$. We now calculate expressions as

$$\mathbb{E}[\cos(2(X_t + \alpha X_{t-\tau} + \beta W_{t-\tau}] = \sum_{n=0}^{\infty} \frac{(-1)^n}{2n!} 2^{2n} \mathbb{E}[\mathbb{E}[(X_t + \alpha X_{t-\tau} + \beta W_{t-\tau})^{2n} | X_0]],$$

$$\mathbb{E}[(X_t + \alpha X_{t-\tau} + \beta W_{t-\tau})^{2n} | X_0] = \sum_{j=0}^{2n} \mathbb{E}[\mathbb{E}[(\alpha X_{t-\tau} + \beta W_{t-\tau})^{2n-j} \mathbb{E}[X_t^j | X_{t-\tau}] | X_0]].$$

The expectations $\mathbb{E}[X_t^j | X_{t-\tau}]$ are given by Eq. (C7). Expanding the term $(\alpha X_{t-\tau} + \beta W_{t-\tau})^{2n-j}$, it becomes obvious we will need terms of the form $Z_{n,l} := \mathbb{E}[X_s^n W_s^l | X_0]$. Using Eq. (C2) gives

$$\mathrm{d}Z_{n,l} = -nkZ_{n,l} + \tfrac{1}{2}(n^2 - n)\gamma^2 Z_{n-2,l} + \tfrac{1}{2}(l^2 - l)Z_{n,l-2} + nl\gamma Z_{n-1,l-1},$$

which can be solved iteratively. In total

$$\begin{aligned}\mathbb{E}[(X_t + \alpha X_{t-\tau} + \beta W_{t-\tau})^{2n} | X_0] = \left(-\frac{1}{2}\right)^n (2n-1)!!\, k^{-n} e^{-kn(2t+\tau)} (\gamma^2 e^{k\tau} + \alpha^2(\gamma^2 e^{3k\tau} - \gamma^2 e^{k(2t+\tau)}) \\ + \alpha(2\gamma^2 e^{2k\tau} + \beta(4\gamma e^{k(t+2\tau)} - 4\gamma e^{k(2t+\tau)}) - 2\gamma^2 e^{2kt}) - 2\beta^2 k(t-\tau)e^{k(2t+\tau)} \\ + \beta(4\gamma e^{k(t+\tau)} - 4\gamma e^{2kt}) - \gamma^2 e^{k(2t+\tau)})^n.\end{aligned}$$

This finally results in

$$\begin{aligned}\mathbb{E}[\cos(X_t + \alpha X_{t-\tau} + \beta W_{t-\tau}) | X_0] = \exp\Bigg(-\frac{\gamma^2}{k}(1 - e^{-2kt}) - \alpha\frac{2\gamma^2}{k} e^{-k\tau}(1 - e^{-2k(t-\tau)}) - \alpha^2\frac{\gamma^2}{k}(1 - e^{-2k(t-\tau)}) \\ - \alpha\beta\frac{4\gamma}{k}(1 - e^{-k(t-\tau)}) - \beta\frac{4\gamma}{k} e^{-k\tau}(1 - e^{-k(t-\tau)}) - \beta^2 2(t-\tau)\Bigg).\end{aligned}$$

APPENDIX D: MULTIQUBIT NOISE

This section proves a result regarding the factoring of fidelity distributions of n-qubit systems, which have a product initial state and evolve under the same noise source.

Lemma D 1 (Factoring fidelity for pure states). Let the state $\psi_{(n)}$ of a n-qubit system evolve according to

$$\mathrm{d}\psi_{(n)} = -iH_n\psi_{(n)}\mathrm{d}t - \tfrac{1}{2}S_n^2\psi_{(n)}\mathrm{d}[X]_t - iS_n\psi_{(n)}\mathrm{d}X_t, \quad \psi_{(n)}(0) = \bigotimes_{j=1}^{n}\psi_{j0},$$

where the Hamiltonian H_n and the noise operator S_n take the sum form

$$H_n = \sum_{j=1}^{n} A_j, \quad A_j = I^{\otimes(j-1)} \otimes \tilde{A}_j \otimes I^{\otimes(n-j)}, \quad \tilde{A}_j = \tilde{A}_j{}^{\dagger},$$

$$S_n = \sum_{j=1}^{n} Q_j, \quad Q_j = I^{\otimes(j-1)} \otimes \tilde{Q}_j \otimes I^{\otimes(n-j)}, \quad \tilde{Q}_j = \tilde{Q}_j{}^{\dagger}.$$

Let $\phi_{(n)}$ be the noiseless target state. Then

$$|\phi_{(n)}^{\dagger}\psi_{(n)}|^2 = \prod_{j=1}^{n} |\phi_j^{\dagger}\psi_j|^2,$$

where ψ_j is a one-qubit state evolving according to the SSE

$$\mathrm{d}\psi_j = -i\tilde{A}_j\psi_j\,\mathrm{d}t - \tfrac{1}{2}\tilde{Q}_j^2\psi_j\,\mathrm{d}[X]_t - i\tilde{Q}_j\psi_j\,\mathrm{d}X_t, \quad \psi_j(0) = \psi_{j0},$$

and ϕ_j is its corresponding noiseless target state.

Proof. Squaring S_n, we find

$$S_n^2 = \sum_{j=1}^{n} Q_j^2 + \sum_{j=1}^{n}\sum_{k\neq j}^{n} Q_{jk}, \quad Q_{jk} = I^{\otimes(j-1)} \otimes \tilde{Q}_j \otimes I^{\otimes(k-j-1)} \otimes \tilde{Q}_k \otimes I^{\otimes(n-k)}.$$

By induction we prove the $\psi_{(n)} = \bigotimes_{j=1}^{n}\psi_j$.

This holds trivially for $n = 1$. Now, assume that the statement holds for n. Then for $n + 1$, we use Itô's formula to obtain

$$\mathrm{d}\bigotimes_{j=1}^{n+1}\psi_j = -iH_{n+1}\bigotimes_{j=1}^{n+1}\psi_j\,\mathrm{d}t - iS_{n+1}\bigotimes_{j=1}^{n+1}\psi_j\,\mathrm{d}X_t - \frac{1}{2}S_{n+1}\bigotimes_{j=1}^{n+1}\psi_j\,\mathrm{d}[X]_t.$$

As we have equal initial conditions, we indeed find $\psi_{(n+1)} = \bigotimes_{j=1}^{n+1}\psi_j$ for all $n \in \mathbb{N}$.

Analogously, we find $\phi_{(n)} = \bigotimes_{j=1}^{n}\phi_j$. For the fidelity, we then deduce

$$|\phi_{(n)}^\dagger\psi_{(n)}|^2 = \phi_{(n)}^\dagger\psi_{(n)}\psi_{(n)}^\dagger\phi_{(n)} = \left(\bigotimes_{j=1}^{n}\phi_j^\dagger\bigotimes_{j=1}^{n}\psi_j\right)\left(\bigotimes_{j=1}^{n}\psi_j^\dagger\bigotimes_{j=1}^{n}\phi_j\right) = \prod_{j=1}^{n}|\phi_j^\dagger\psi_j|^2.$$

■

Note that these results do not only hold for qubits but for any finite ensemble of finite dimensional quantum systems.

APPENDIX E: STOCHASTIC INTEGRATION

Numerical verification of the analytic results is performed using stochastic integration. To solve for the noise and state simultaneously, we define $\mathsf{Y} := (\psi, X)$. For the OU process, this gives the differential equation

$$\mathrm{d}\mathsf{Y} = a(\mathsf{Y})\,\mathrm{d}t + b(\mathsf{Y})\,\mathrm{d}W_t, \quad a(\mathsf{Y}) = \left(\begin{array}{c|c} -iH + ikXS - \frac{\gamma^2}{2}S^\dagger S & \mathbf{0} \\ \hline \mathbf{0}^{\mathrm{T}} & -k \end{array}\right)\mathsf{Y}, \quad b(\mathsf{Y}) = \left(\begin{array}{c|c} -i\gamma S & \mathbf{0} \\ \hline \mathbf{0}^{\mathrm{T}} & \frac{1}{X} \end{array}\right)\mathsf{Y}.$$

These equations can be solved discretely over time steps Δt using a numerical integration scheme. One possible scheme is the explicit (weak) first-order Euler-Maruyama scheme [71] as

$$\mathsf{Y}_{n+1} = \mathsf{Y}_n + a(\mathsf{Y}_n)\Delta t + b(\mathsf{Y}_n)\mathcal{N}\sqrt{\Delta t},$$

where $\mathcal{N}$ is a standard normal distribution. Throughout this work, convergence issues persisted using stochastic integration schemes for OU noise at higher evolution times, likely due to the non-Lipschitz $1/X$ dependence [61] and possibly the non-Euclidean space in which the states live. These convergence issues are absent for white noise and always occur below fidelities of $F = 0.95$, which is not a relevant regime for pragmatic quantum computing and, therefore, is not a deliberating issue. We have found that these issues are mitigated (but not resolved) when using a higher-order scheme such as the explicit (weak) second-order scheme due to Platen [60,61], which is used throughout this work. This scheme is given by

$$\mathsf{Y}_{n+1} = \mathsf{Y}_n + \tfrac{1}{2}(a(\bar{\Upsilon}) + a(\mathsf{Y}_n))\Delta t + \tfrac{1}{4}(b(\bar{\Upsilon}^+) + b(\bar{\Upsilon}^-) + 2b(\mathsf{Y}_n))\mathcal{N}\sqrt{\Delta t} + \tfrac{1}{4}(b(\bar{\Upsilon}^+) - b(\bar{\Upsilon}^-))(\mathcal{N}^2 - 1)\sqrt{\Delta t},$$

with supporting values $\bar{\Upsilon} = \mathsf{Y}_n + a(\mathsf{Y}_n)\Delta t + b(\mathsf{Y}_n)\mathcal{N}\sqrt{\Delta t}$ and $\bar{\Upsilon}^\pm = \mathsf{Y}_n + a(\mathsf{Y}_n)\Delta t \pm b(\mathsf{Y}_n)\sqrt{\Delta t}$.

APPENDIX F: SECOND-ORDER PAULI APPROXIMATION

For the second-order results as in Fig. 3, the closed system for the vector V

$$\mathsf{V} = [|\phi^\dagger\psi|^2, |\phi^\dagger S\psi|^2, X(t)(\phi^\dagger S\psi\psi^\dagger\phi - \phi^\dagger\psi\psi^\dagger S\phi), X^2(t)|\phi^\dagger\psi|^2, X^2(t)|\phi^\dagger S\psi|^2, X^3(t)(\phi^\dagger S\psi\psi^\dagger\phi - \phi^\dagger\psi\psi^\dagger S\phi)],$$

is found to be

$$\dot{\mathsf{V}} = \begin{bmatrix} -\gamma^2 & \gamma^2 & ik & 0 & 0 & 0 \\ \gamma^2 & -\gamma^2 & -ik & 0 & 0 & 0 \\ -2i\gamma^2 & 2i\gamma^2 & -(k+2\gamma^2) & 2ik & -2ik & 0 \\ \gamma^2 & 0 & -2i\gamma^2 & -(2k+\gamma^2) & \gamma^2 & ik \\ 0 & \gamma^2 & 2i\gamma^2 & \gamma^2 & -(2k+\gamma^2) & -ik \\ 0 & 0 & 2\gamma^2 & 2i\big(k\mathbb{E}\big[X_t^2\big] - 2\gamma^2\big) & -2i\big(k\mathbb{E}\big[X_t^2\big] - 2\gamma^2\big) & -(3k+2\gamma^2) \end{bmatrix}\mathsf{V}, \quad \mathsf{V}(0) = \begin{bmatrix} 1 \\ \mathsf{S}_0^2 \\ 0 \\ 0 \\ 0 \\ 0 \end{bmatrix},$$

with $\mathsf{S}_0 = \phi_0^\dagger S\phi_0$. This system is solved numerically to retrieve the expectation of the fidelity.

APPENDIX G: NONCOMMUTING HAMILTONIANS

For the noncommuting system we consider $H = \alpha\sigma_1$, $S = \sigma_2$, giving $[H, S] = 2i\alpha\sigma_3$, where $\{\sigma_1, \sigma_2, \sigma_3\}$ can be any cyclic permutation of $\{\sigma_X, \sigma_Y, \sigma_Z\}$. The group structure of the Pauli matrices allows us to close the system of SDEs for the vector

$$\mathsf{V} = \begin{bmatrix} \mathsf{F} \\ |\phi^\dagger\sigma_1\psi|^2 \\ |\phi^\dagger\sigma_2\psi|^2 \\ |\phi^\dagger\sigma_3\psi|^2 \\ i(\phi^\dagger\sigma_1\psi\psi^\dagger\phi - \phi^\dagger\psi\psi^\dagger\sigma_1\phi) \\ i(\phi^\dagger\sigma_2\psi\psi^\dagger\phi - \phi^\dagger\psi\psi^\dagger\sigma_2\phi) \\ i(\phi^\dagger\sigma_3\psi\psi^\dagger\phi - \phi^\dagger\psi\psi^\dagger\sigma_3\phi) \\ \phi^\dagger\sigma_2\psi\psi^\dagger\sigma_1\phi + \phi^\dagger\sigma_1\psi\psi^\dagger\sigma_2\phi \\ \phi^\dagger\sigma_3\psi\psi^\dagger\sigma_1\phi + \phi^\dagger\sigma_1\psi\psi^\dagger\sigma_3\phi \\ \phi^\dagger\sigma_3\psi\psi^\dagger\sigma_2\phi + \phi^\dagger\sigma_2\psi\psi^\dagger\sigma_3\phi \end{bmatrix} \in \mathbb{R}^{10}.$$

We find that the matrix A splits in a commutator part A_c and a noise part B^2, resulting in the system

$$\mathrm{d}\mathsf{V} = \alpha A_c \mathsf{V}\,\mathrm{d}t + \tfrac{1}{2}\gamma^2 B^2 \mathsf{V}\,\mathrm{d}t + B\mathsf{V}\,\mathrm{d}X_t,$$

with

$$A_c = \begin{bmatrix} 0&0&0&0&0&0&0&0&0&0 \\ 0&0&0&0&0&0&0&0&0&0 \\ 0&0&0&0&0&0&0&0&0&-2 \\ 0&0&0&0&0&0&0&0&0&2 \\ 0&0&0&0&0&0&0&0&0&0 \\ 0&0&0&0&0&0&-2&0&0&0 \\ 0&0&0&0&0&2&0&0&0&0 \\ 0&0&0&0&0&0&0&0&-2&0 \\ 0&0&0&0&0&0&0&2&0&0 \\ 0&0&4&-4&0&0&0&0&0&0 \end{bmatrix}, \qquad B = \begin{bmatrix} 0&0&0&0&0&-1&0&0&0&0 \\ 0&0&0&0&0&0&0&0&1&0 \\ 0&0&0&0&0&1&0&0&0&0 \\ 0&0&0&0&0&0&0&0&-1&0 \\ 0&0&0&0&0&0&1&-1&0&0 \\ 2&0&-2&0&0&0&0&0&0&0 \\ 0&0&0&0&-1&0&0&0&0&-1 \\ 0&0&0&0&1&0&0&0&0&1 \\ 0&-2&0&2&0&0&0&0&0&0 \\ 0&0&0&0&0&0&1&-1&0&0 \end{bmatrix}.$$

Solving this system as in Sec. II B 1 is not possible since $[A_c, B] \neq 0$. However, a perturbation technique can be used when the Hamiltonian strength is much larger than the noise, i.e., $\varepsilon^2 := \gamma^2/\alpha \ll 1$, which holds for many realistic systems. Rescaling time $\widehat{t} = t/\alpha$, we obtain a rescaled system of equations for $\widehat{\mathsf{V}} = \mathsf{V}_{t/\alpha}$ and $\widehat{X} = X_{t/\alpha}$,

$$\mathrm{d}\widehat{\mathsf{V}} = A_c\widehat{\mathsf{V}}\,\mathrm{d}\widehat{t} + \tfrac{1}{2}\varepsilon^2 B^2\widehat{\mathsf{V}}\,\mathrm{d}\widehat{t} + B\widehat{\mathsf{V}}\,\mathrm{d}\widehat{X}_t,$$

where $\widehat{X}$ has the quadratic variation $[\widehat{X}]_{\widehat{t}} = \varepsilon^2\widehat{t}$.

In the following, we assume without loss of generality that $\alpha = 1$ and $\gamma^2 \ll 1$. Otherwise, we simply rescale time as above and write V instead of $\widehat{\mathsf{V}}$. Setting $\mathsf{U} := \exp(-A_c t)\mathsf{V}$ to get

$$\mathrm{d}\mathsf{U} = \tfrac{1}{2}\gamma^2 D^2(t)\mathsf{U}\,\mathrm{d}t + D(t)\mathsf{U}\,\mathrm{d}X_t, \tag{G1}$$

with

$$D(t) = \exp(-A_c t)B\exp(A_c t) = \cos(2t)B - \tfrac{1}{2}\sin(2t)[A_c, B],$$

where the second equality can be established according to a generalized harmonic oscillator [72]. Although (G1) cannot be solved explicitly, an approximation to its solution can be found via the stochastic Magnus expansion [58], which states that

$$\mathsf{U} = \exp(\mathsf{L}) = \exp\left(\sum_{n,r}\gamma^{2n-r}\mathsf{L}^{(r,n-r)}\right),$$

where $\mathsf{L}^{(r,n-r)}$ are the expansion terms up to order γ^2 in L. For general processes, we find

$$\mathsf{U}_t = \exp\left(\int_0^t D(s)\,\mathrm{d}X_s + O(\gamma^3)\right),$$

which, for WN, gives

$$\mathbb{E}[\mathsf{U}_t] \approx \exp\left(\frac{\gamma^2}{2}\int_0^t D^2(s)\,ds\right).$$

For the fidelity under white noise, we then obtain the approximation

$$\mathsf{F}_t = \mathbb{E}[\mathsf{U}_t] \approx \tfrac{1}{2} + \tfrac{1}{2}\,\mathsf{C}_1^2 e^{-2\gamma^2 t} + \tfrac{1}{2} e^{-\gamma^2 t}\big(\sinh(u)\big(\big(\mathsf{C}_2^2 - \mathsf{C}_3^2\big)\cos(2at) - 2\mathsf{C}_2\mathsf{C}_3\sin(2at)\big) + \big(\mathsf{C}_2^2 + \mathsf{C}_3^2\big)\cosh(u)\big).$$

with $u = \gamma^2 \sin(2\alpha t)/2\alpha$. For the OU process with $k > 0$, the exponential cannot be expressed analytically. Instead, one could approximate it by expanding the exponential up to the second order to find

$$\mathbb{E}[\mathsf{U}_t] \approx I + \frac{\gamma^2}{2}\int_0^t D^2(s)ds - \frac{\gamma^2}{2}k\int_0^t \left\{e^{-ks}D(s), \int_0^s e^{ks'}D(s')ds'\right\}ds + \frac{\gamma^2}{4}k\int_0^t \left\{e^{-2ks}D(s), \int_0^s e^{2ks'}D(s')ds'\right\}ds.$$

[1] J. Preskill, Quantum computing in the NISQ era and beyond, Quantum **2**, 79 (2018).

[2] M. L. Day, P. J. Low, B. White, R. Islam, and C. Senko, Limits on atomic qubit control from laser noise, npj Quantum Inf. **8**, 72 (2022).

[3] H. Nakav, R. Finkelstein, L. Peleg, N. Akerman, and R. Ozeri, Effect of fast noise on the fidelity of trapped-ion quantum gates, Phys. Rev. A **107**, 042622 (2023).

[4] L.-L. Yan, J.-Q. Zhang, J. Jing, and M. Feng, Suppression of dissipation in a laser-driven qubit by white noise, Phys. Lett. A **379**, 2417 (2015).

[5] M. Mohan, R. de Keijzer, and S. Kokkelmans, Robust control and optimal Rydberg states for neutral atom two-qubit gates, Phys. Rev. Res. **5**, 033052 (2023).

[6] S. Jandura, J. D. Thompson, and G. Pupillo, Optimizing Rydberg gates for logical-qubit performance, PRX Quantum **4**, 020336 (2023).

[7] C. A. Brasil, F. F. Fanchini, and R. d. J. Napolitano, A simple derivation of the Lindblad equation, Rev. Bras. Ensino Fís. **35**, 01 (2013).

[8] D. Manzano, A short introduction to the Lindblad master equation, AIP Adv. **10**, 025106 (2020).

[9] P. Welch, The use of fast Fourier transform for the estimation of power spectra: A method based on time averaging over short, modified periodograms, IEEE Trans. Audio Electroacoust. **15**, 70 (1967).

[10] M. A. Nielsen and I. L. Chuang, *Quantum Computation and Quantum Information* (Cambridge University Press, Cambridge, 2010).

[11] K. Jacobs, *Quantum Measurement Theory and Its Applications* (Cambridge University Press, Cambridge, UK, 2014).

[12] J. Preskill, Quantum Shannon theory, arXiv:1604.07450.

[13] T. O'Brien, B. Tarasinski, and L. DiCarlo, Density-matrix simulation of small surface codes under current and projected experimental noise, npj Quantum Inf. **3**, 39 (2017).

[14] J. Sun, X. Yuan, T. Tsunoda, V. Vedral, S. C. Benjamin, and S. Endo, Mitigating realistic noise in practical noisy intermediate-scale quantum devices, Phys. Rev. Appl. **15**, 034026 (2021).

[15] R. Carballeira, D. Dolgitzer, P. Zhao, D. Zeng, and Y. Chen, Stochastic Schrödinger equation derivation of non-Markovian two-time correlation functions, Sci. Rep. **11**, 11828 (2021).

[16] C. Gardiner and P. Zoller, *Quantum Noise: A Handbook of Markovian and Non-Markovian Quantum Stochastic Methods with Applications to Quantum Optics*, Springer Series in Synergetics (Springer, Berlin, 2004).

[17] H.-P. Breuer, Non-Markovian generalization of the Lindblad theory of open quantum systems, Phys. Rev. A **75**, 022103 (2007).

[18] M. Moodley and F. Petruccione, Stochastic wave-function unraveling of the generalized Lindblad master equation, Phys. Rev. A **79**, 042103 (2009).

[19] A. Barchielli, C. Pellegrini, and F. Petruccione, Stochastic Schrödinger equations with coloured noise, Europhys. Lett. **91**, 24001 (2010).

[20] H.-P. Breuer and J. Piilo, Stochastic jump processes for non-Markovian quantum dynamics, Europhys. Lett. **85**, 50004 (2009).

[21] F. Chapeau-Blondeau, Modeling and simulation of a quantum thermal noise on the qubit, Fluct. Noise Lett. **21**, 2250060 (2022).

[22] S. Simbierowicz, M. Borrelli, V. Monarkha, V. Nuutinen, and R. E. Lake, Inherent thermal-noise problem in addressing qubits, PRX Quantum **5**, 030302 (2024).

[23] E. Vlachos, H. Zhang, V. Maurya, J. Marshall, T. Albash, and E. M. Levenson-Falk, Master equation emulation and coherence preservation with classical control of a superconducting qubit, Phys. Rev. A **106**, 062620 (2022).

[24] G. Di Bartolomeo, M. Vischi, F. Cesa, R. Wixinger, M. Grossi, S. Donadi, and A. Bassi, Noisy gates for simulating quantum computers, Phys. Rev. Res. **5**, 043210 (2023).

[25] R. de Keijzer, O. Tse, and S. Kokkelmans, Pulse based variational quantum optimal control for hybrid quantum computing, Quantum **7**, 908 (2023).

[26] O. R. Meitei, B. T. Gard, G. S. Barron, D. P. Pappas, S. E. Economou, E. Barnes, and N. J. Mayhall, Gate-free state preparation for fast variational quantum eigensolver simulations, npj Quantum Inf. **7**, 155 (2021).

[27] B. Li, S. Ahmed, S. Saraogi, N. Lambert, F. Nori, A. Pitchford, and N. Shammah, Pulse-level noisy quantum circuits with QuTiP, Quantum **6**, 630 (2022).

[28] I. Semina, V. Semin, F. Petruccione, and A. Barchielli, Stochastic schrödinger equations for Markovian and non-Markovian cases, Open Syst. Inf. Dynam. **21**, 1440008 (2014).

[29] X. Jiang, J. Scott, M. Friesen, and M. Saffman, Sensitivity of quantum gate fidelity to laser phase and intensity noise, Phys. Rev. A **107**, 042611 (2023).

[30] M. M. Müller, S. Gherardini, T. Calarco, S. Montangero, and F. Caruso, Information theoretical limits for quantum optimal control solutions: Error scaling of noisy control channels, Sci. Rep. **12**, 21405 (2022).

[31] M. Otten, K. Kapoor, A. B. Özgüler, E. T. Holland, J. B. Kowalkowski, Y. Alexeev, and A. L. Lyon, Impacts of noise and structure on quantum information encoded in a quantum memory, Phys. Rev. A **104**, 012605 (2021).

[32] V. Semin, Non-Markovian generalization of a stochastic Schrödinger equation for two interacting qubits, Europhys. Lett. **130**, 10003 (2020).

[33] K. Kobayashi and N. Yamamoto, Control limit on quantum state preparation under decoherence, Phys. Rev. A **99**, 052347 (2019).

[34] X. Li, Markovian embedding procedures for non-Markovian stochastic Schrödinger equations, Phys. Lett. A **387**, 127036 (2021).

[35] Q. Huang and M. Merkli, Qubit dynamics with classical noise, Phys. Open **5**, 100043 (2020).

[36] Y. Ouyang, D. R. White, and E. T. Campbell, Compilation by stochastic Hamiltonian sparsification, Quantum **4**, 235 (2020).

[37] T. J. Green, J. Sastrawan, H. Uys, and M. J. Biercuk, Arbitrary quantum control of qubits in the presence of universal noise, New J. Phys. **15**, 095004 (2013).

[38] In this work, we choose to refrain from using standard bra-ket notation for readability purposes.

[39] G. Lawler, *Introduction to Stochastic Calculus with Applications* (Taylor & Francis, London, 2016).

[40] D. Kulasiri and W. Verwoerd, A brief review of mathematical background, in *Stochastic Dynamics*, North-Holland Series in Applied Mathematics and Mechanics, Vol. 44, edited by D. Kulasiri and W. Verwoerd (North-Holland, Amsterdam, 2002), pp. 27–68.

[41] O. D. Street and D. Crisan, Semi-martingale driven variational principles, Proc. R. Soc. Lond. A **477**, 20200957 (2021).

[42] E. Wong, Representation of martingales, quadratic variation and applications, SIAM J. Control **9**, 621 (1971).

[43] H. Hasegawa and H. Ezawa, Stochastic calculus and some models of irreversible processes, Prog. Theor. Phys. Suppl. **69**, 41 (1980).

[44] L. Bouten, M. Guta, and H. Maassen, Stochastic Schrödinger equations, J. Phys. A: Math. Gen. **37**, 3189 (2004).

[45] V. V. Ignatyuk and V. G. Morozov, Master equation for open quantum systems: Zwanzig-Nakajima projection technique and the intrinsic bath dynamics, arXiv:1911.12312.

[46] M. Morgado and S. Whitlock, Quantum simulation and computing with Rydberg-interacting qubits, AVS Quantum Sci. **3**, 023501 (2021).

[47] M. H. Devoret, A. Wallraff, and J. M. Martinis, Superconducting qubits: A short review, arXiv:cond-mat/0411174.

[48] E. Paladino, Y. M. Galperin, G. Falci, and B. L. Altshuler, 1/f noise: Implications for solid-state quantum information, Rev. Mod. Phys. **86**, 361 (2014).

[49] P. Groszkowski, A. Seif, J. Koch, and A. A. Clerk, Simple master equations for describing driven systems subject to classical non-Markovian noise, Quantum **7**, 972 (2023).

[50] S. Weinberg, Lindblad decoherence in atomic clocks, Phys. Rev. A **94**, 042117 (2016).

[51] P. W. Milonni, *An Introduction to Quantum Optics and Quantum Fluctuations* (Oxford University Press, Oxford, 2019).

[52] F. Hooge and P. Bobbert, On the correlation function of 1/f noise, Phys. B: Condens. Matter **239**, 223 (1997).

[53] X.-J. Lu, A. Ruschhaupt, and J. G. Muga, Fast shuttling of a particle under weak spring-constant noise of the moving trap, Phys. Rev. A **97**, 053402 (2018).

[54] V. Bareikis and R. Katilius, *Noise in Physical Systems and 1/f Fluctuations* (World Scientific, Singapore, 1995).

[55] M. A. Johnson and M. H. Moradi, *PID Control* (Springer, Berlin, 2005).

[56] A. Vepsäläinen, R. Winik, A. H. Karamlou, J. Braumüller, A. D. Paolo, Y. Sung, B. Kannan, M. Kjaergaard, D. K. Kim, A. J. Melville, B. M. Niedzielski, J. L. Yoder, S. Gustavsson, and W. D. Oliver, Improving qubit coherence using closed-loop feedback, Nat. Commun. **13**, 1932 (2022).

[57] A. Armaroli, G. Dujardin, A. Kudlinski, A. Mussot, S. Trillo, S. De Bièvre, and M. Conforti, Stochastic modulational instability in the nonlinear Schrödinger equation with colored random dispersion, Phys. Rev. A **105**, 013511 (2022).

[58] K. Kamm, S. Pagliarani, and A. Pascucci, On the stochastic magnus expansion and its application to spdes, J. Sci. Comput. **89**, 56 (2021).

[59] K. Wintersperger, F. Dommert, T. Ehmer, A. Hoursanov, J. Klepsch, W. Mauerer, G. Reuber, T. Strohm, M. Yin, and S. Luber, Neutral atom quantum computing hardware: Performance and end-user perspective, EPJ Quantum Technol. **10**, 32 (2023).

[60] H.-P. Breuer, U. Dorner, and F. Petruccione, Numerical integration methods for stochastic wave function equations, Comput. Phys. Commun. **132**, 30 (2000).

[61] P. E. Kloeden and E. Platen, *Numerical Solution of Stochastic Differential Equations* (Springer, Berlin, 1999).

[62] S. de Léséleuc, D. Barredo, V. Lienhard, A. Browaeys, and T. Lahaye, Analysis of imperfections in the coherent optical excitation of single atoms to Rydberg states, Phys. Rev. A **97**, 053803 (2018).

[63] F. Wudarski, Y. Zhang, A. N. Korotkov, A. Petukhov, and M. Dykman, Characterizing low-frequency qubit noise, Phys. Rev. Appl. **19**, 064066 (2023).

[64] All systems of ordinary differential equations are solved using the `odeint` methods from SciPy [73].

[65] B. Øksendal, *Stochastic Differential Equations*, Universitext (Springer, Berlin, 2010).

[66] Weglarczyk, Stanislaw, Kernel density estimation and its application, ITM Web Conf. **23**, 00037 (2018).

[67] Y. Zhao, R. Zhang, W. Chen, X.-B. Wang, and J. Hu, Creation of Greenberger-Horne-Zeilinger states with thousands of atoms by entanglement amplification, npj Quantum Inf. **7**, 24 (2021).

[68] E. R. Bittner, H. Li, S. A. Shah, C. Silva, and A. Piryatinski, Correlated noise enhances coherence and fidelity in coupled qubits, arXiv:2308.00841.

[69] All data and code used are available publicly from https://gitlab.tue.nl/s1658271/sse.git.

[70] S. Särkkä and A. Solin, *Applied Stochastic Differential Equations*, Institute of Mathematical Statistics Textbooks (Cambridge University Press, Cambridge, UK, 2019).

[71] M. Bayram, T. Partal, and G. Orucova Buyukoz, Numerical methods for simulation of stochastic differential equations, Adv. Differ. Eq. **2018**, 17 (2018).

[72] K. R. Parthasarathy, *An Introduction to Quantum Stochasticcalculus* (Birkhäuser, Basel, 1992).

[73] P. Virtanen and SciPy 1.0 Contributors, SciPy 1.0: Fundamental algorithms for scientific computing in Python, Nat. Methods **17**, 261 (2020).